

## **ACTIVE FAULTING AND STRESS REDISTRIBUTIONS IN THE DIXIE VALLEY, BEOWAWE, AND BRADYS GEOTHERMAL FIELDS: IMPLICATIONS FOR GEOTHERMAL EXPLORATION IN THE BASIN AND RANGE**

S. John Caskey

Department of Geosciences  
San Francisco State University  
1600 Holloway Ave.  
San Francisco, CA 94132, USA  
caskey@sfsu.edu

Steven G. Wesnousky

Center for Neotectonic Studies  
University of Nevada  
Reno, NV 89557, USA  
steve@seismo.unr.edu

### **ABSTRACT**

Detailed and preliminary field investigations delineating the most recent fault ruptures in vicinity of the Dixie Valley, Beowawe, and Bradys geothermal fields allow an assessment of static stress changes and their possible influences on the geothermal environments. Our models for the Dixie Valley and Beowawe regions show increased failure stress on faults and fractures associated with the geothermal reservoirs with contributions from both increased shear stress and decreased fault-normal stress. These stress changes are especially pronounced for the Dixie Valley geothermal field where large increases in failure stress are concentrated between Holocene rupture endpoints. The portion of the fault with the most enhanced tensile stresses lies at shallow crustal levels between the northern and southern limits of the production field. The sense of stress changes from both Holocene and historic fault ruptures in Dixie Valley are consistent with recent borehole studies of in situ stress and fracture permeability which show the Dixie Valley fault and fault-parallel fractures are critically stressed for failure and hydraulically conductive within the geothermal field. Structural relations in the Bradys geothermal field are analogous to the relations in Dixie Valley, and we suspect that a similar sense of stress change has influenced the Bradys geothermal environment. Our investigation shows that induced stress concentrations at the endpoints of normal fault ruptures may promote

favorable conditions for hydrothermal activity. This may be accomplished in two ways: 1) Nearby fault ruptures may induce aftershocks associated with small amounts of slip on macro fractures along the fault and within the damage zone of the fault, thereby producing open fractures without producing large stress drops on the fault; and 2) If the geothermal field is adjacent to fault rupture endpoints, then it is conceivable that decreases in fault-normal stress may be large enough to produce significant increases in fracture dilatancy, thereby increasing hydraulic conductivity. Our studies illustrate that a detailed understanding of the neotectonic framework and the mechanics of faulting processes are fundamental to developing conceptual models for controls on the state of stress and fracture permeability in geothermal fields.

### **INTRODUCTION**

It is widely accepted that geothermal activity is largely associated with areas of active faulting. Figure 1 illustrates that the spatial correlation between thermal springs and late Quaternary faults in Nevada is quantitatively robust. It is commonly accepted that faults play a role in this association by sometimes forming conduits for upward movement of ground water. Similarly, in geothermal reservoirs, it is thought that it is necessary to have recent fault movements in order to maintain open fractures and permeability. However, the question of how the mechanics of the faulting process may play a causative role in the factors that influence geothermal

production remains poorly understood. A better understanding of the faulting processes that create and maintain reservoir permeability can potentially reduce geothermal exploration costs if it can be used to more accurately target successful wells. With this objective in mind we have initiated detailed field studies of active faults in the Dixie Valley (Oxbow Geothermal Corp.), Beowawe (Oxbow Power of Beowawe), and Bradys (Florida Power and Light) geothermal production fields to characterize the distribution and recency of fault movements. To evaluate how the mechanics of the faulting process may influence the geothermal environment, we examine the redistribution of stresses associated with the most recent identifiable fault ruptures in the vicinity of the geothermal fields.

## **METHOD AND FAULT MODELS**

We use the approach of Reasenber and Simpson (1992) and Stein *et al.* (1992), based on the methodology of Okada (1992), to calculate the static stress changes resulting from displacements on individual fault segments (i.e. dislocations) embedded in an elastic half space. Individual fault ruptures are identified from aerial photos and field verification. Average displacements on faults are based on profiles and field measurements of vertical offsets across fault scarps. The values of static stress changes are then used to calculate the Coulomb Failure Function (CFF) (failure stress changes) on the faults associated with the geothermal fields, where CFF is defined as

$$CFF = \Delta\tau_S + \mu(\Delta\sigma_n),$$

where  $\Delta\tau_S$  is the static shear stress change (positive in the direction of fault slip),  $\Delta\sigma_n$  is the normal stress change (positive for tensile stress changes), and  $\mu$  is the coefficient of static friction. Possible changes in pore fluid pressure are not considered in the stress calculations. Stress changes moving a fault closer to failure are reflected by positive values of CFF. CFF values are calculated for an assumed dip slip sense of shear (i.e. rake = -90°). In order to evaluate the relative contributions of shear and normal stress changes to CFF values, we determined CFF for  $\mu = 0.0$  (where only  $\Delta\tau_S$  affects CFF) and  $\mu = 0.40-0.75$  (consistent with laboratory rock mechanics experiments (Byerlee, 1978)). For Dixie Valley calculations, normal stress contributions were determined by subtracting the shear stress changes from the total CFF values.

## **RESULTS**

### **Dixie Valley Geothermal Field**

"The Dixie Valley Geothermal Field (DVGF) is, in many respects, the classic Basin and Range geothermal reservoir developed along an active major range-front fault" (Benoit, 1995). It is located along the southeast-dipping Dixie Valley fault and within the Stillwater Seismic Gap (Wallace and Whitney, 1984); a 45 km-long section of the fault between the 1915 (M7.7) Pleasant Valley and 1954 (M6.8) Dixie Valley earthquake rupture zones to the north and south, respectively (Figure 2). Within the Stillwater Gap, Wallace and Whitney (1984) recognized discontinuous Holocene fault scarps along the Stillwater range front, and they interpreted this to mean that the gap has experienced at least one large Holocene earthquake. Our field studies of these surface ruptures indicate that ruptures to the north and south of the DVGF are likely of different ages and that the geothermal field lies within a ~10 km gap with respect to these Holocene earthquake ruptures. For example, profiles of fault scarps north of the DVGF are generally more degraded with shallower scarp slope angles compared with those to the south, indicating an older age of formation (Figure 3). Fault scarps to the south, with few exceptions, exhibit steep scarp slope angles, essentially at angle of repose (~30°) for unconsolidated alluvial fan gravel deposits. Our interpretation of different ages for these scarps is in agreement with previous, more detailed scarp profile analyses of Pearthree (1990) for the Dixie Valley region. There is no evidence for Holocene fault ruptures along the 10 km portion of the range front in the vicinity of the DVGF. It is possible that the lack of scarps in the DVGF is a result of non-preservation due to erosion and/or burial of scarps. However, several landslides and fan surfaces along the range front interpreted to be pre-Holocene in age are apparently not faulted, indicating that this portion of the range front has not ruptured at the surface in the Holocene.

Holocene fault ruptures south of the DVGF overlap with the 1954 Dixie Valley rupture zone by 22 km and can be traced northward for a distance of 45 km, to ~5 km south of the DVGF. The interpreted older Holocene scarps can be traced from ~4 km north of the DVGF to the Sou Hills (Figure 2). The age of fault ruptures south of the DVGF is constrained from field relations. Faulted alluvial fan deposits in the Stillwater Gap area contain or overly Mazama tephra (~7 ka) at two locations (Caskey et. al, 1996; work in preparation). Unfaulted fan deposits along the southern portion of the rupture zone contain Turupah

Flat tephra (1.5 ka) (Bell and Katzer, 1990). Hence, the absolute age of faulting is bracketed as 7 ka-1.5 ka. Similarly, Pearthree's (1990) analyses of scarp profiles suggest that these scarps may be as young as 2 ka. Presently, we have no absolute age control on Holocene scarps north of the DVGF. However, Pearthree's (1990) profile analyses indicate that these fault ruptures may be several thousand years older than those south of the DVGF. The observations indicating that scarps north and south of DVGF appear to represent different aged events gives us confidence that the ~10 km gap we observe between Holocene ruptures may be real rather than a consequence of non-preservation.

The possibility that the DVGF lies between the endpoints of recent earthquake ruptures has important implications for the redistribution of stresses and their influence on geothermal activity in the DVGF. Our model of stress changes associated with Holocene fault ruptures in the Stillwater Gap (Figure 4) suggests that the Dixie Valley fault and parallel fractures in the vicinity of the DVGF have experienced large positive stress changes (>10 bars). The plot of CFF calculations on a horizontal plane at 5 km depth (Figure 4) shows that the large stress changes in the DVGF are due to its proximity to the endpoints of Holocene fault ruptures to the north and south. Stress changes on an inclined grid, oriented 040° 50°SE and projected to down-dip lengths of 6 km (Figure 5), show stress calculations resolved on the Dixie Valley fault plane as well as proximal, fault-parallel fractures. The three panels in Figure 5 represent the total CFF values (Figure 5a), CFF contributions from shear stress changes (Figure 5b), and CFF contributions from normal stress changes only (Figure 5c). Also shown on Figure 5 are locations and depths to the geothermal reservoir for the northern- and southernmost producing wells within the DVGF (Wells 45-33 and 76A-7, respectively). The models show that CFF values within the DVGF largely result from a decrease in normal stresses (i.e. increase in tensile stresses) (compare Figure 5b and 5c), although a significant increase in shear stress is also evident. The DVGF production area lies above the deepest part of the lobe of decreased normal stress. The model may have important implications for recent borehole studies of in situ stress and fracture conductivity (e.g. Barton et al., 1996; Hickman et al., 1997), as well as the dynamics of fluid flow within the DVGF (discussed below).

An examination of CFF values in the Stillwater Gap associated with slip on historic ruptures along the west-dipping 1915 (M7.7) Pleasant Valley and the east-dipping 1954 (M6.8) Dixie Valley rupture zones

(Figure 2) yields similar results for the DVGF, although the stress change values from historic slip are considerably lower in the geothermal field (Figure 6). This is due to the greater distance of the geothermal field from the endpoints of the historic fault ruptures. The plot of CFF calculations, on a horizontal plane at 8 km depth (Figure 6), shows that failure stress along the Dixie Valley fault has everywhere been enhanced in the Stillwater Gap, with most of the fault showing an increase of stress of 1-3 bars. As expected, much larger stress changes occur at the north and south ends of the Gap (>5 bars) near the rupture endpoints. In the fault plane views of the Stillwater Gap segment of the fault (Figure 7) it is clear that stress changes from the 1915 rupture zone are more pronounced in the shallow crust. This is because the Dixie Valley fault and the Pleasant Valley ruptures dip oppositely, and down dip portions of the Dixie Valley fault become increasingly farther from the 1915 ruptures. The fault plane views also show that the historic stress changes in the DVGF result from nearly equal contributions of increased shear stress and decreased normal stress. Although smaller in value to those stress changes associated with Holocene ruptures, the sense of stress change in the DVGF from historic earthquakes is very similar, and therefore would contribute likewise to the state of stress and hydraulic conductivity along the fault.

Mapping along fault scarps in the piedmont area south of the Sou Hills (Figure 2) revealed a small, localized 0.10-0.15 m-high scarp in recent alluvial deposits. The well-preserved nature of such a subtle feature indicates that the scarp is probably historic, and therefore, likely formed during the nearby 1915 earthquake. It may not be a coincidence that the scarp lies within the pronounced lobe of CFF values that result from slip along the 1915 ruptures (Figure 7). The likelihood that the scarp represents a previously unrecognized 1915 rupture appears to demonstrate that stress changes associated with the 1915 earthquake were large enough to trigger fault slip in northern Dixie Valley.

### **Beowawe Geothermal Field**

The Beowawe Geothermal Field (BGF) lies in a more complex structural setting than the DVGF and, at present, has not been field investigated with respect to fault activity to the extent of the Stillwater Gap. However, aerial photo analysis and field reconnaissance mapping during Summer 1999 have resulted in a first order assessment of the distribution and relative ages of the most recently active faults in the vicinity of the BGF.

The Beowawe facility is located within Whirlwind Valley, a small reentrant valley that sits within the Shoshone Range (Figure 8). The west flanks of the Shoshone Range, Dry Hills, and the Cortez Range are each bounded by active faults. The east boundary of Whirlwind Valley is marked by a sharp escarpment which is clearly produced and controlled by the Malpais fault zone. However, it is only along the northern portion of the escarpment that we have observed fault scarps in Quaternary alluvium. These appear to be late Pleistocene to early Holocene-aged scarps based on the estimated age of the youngest alluvial fan deposits offset along the fault. The southernmost limit of observed alluvial scarps along the Malpais fault is approximately 3 km northeast of the town of Beowawe, where we measured vertical offsets of 0.7 m across the scarp. Curiously, the apparent southern limit of surface faulting corresponds to the location of local hot springs along the fault.

Structural relations along the southern portions of the Malpais fault in the BGF were most recently investigated by Benoit (1995), who similarly reported an absence of recent scarps. The age of surface faulting along the southern section of the fault appears to predate Quaternary landslide deposits and adjacent bedrock slump blocks approximately 5 km west of the geysers. These landslide deposits are apparently not faulted; an observation supported by mapping in the area by Smith et al. (1979). Future efforts will focus on placing firmer constraints on the ages of the oldest, unfaulted Quaternary deposits along the southern portion of the Malpais fault, and the age of surface faulting along the northern portion of the fault.

Structural and stratigraphic relations along the west flank of the Shoshone Range (Figure 8) indicate multiple Quaternary faulting events. We interpret the most recent event as being early to mid-Holocene in age based on the estimated age of the youngest, faulted alluvial fan deposits at the mouth of Mt. Lewis Canyon. In this area, older fan deposits exhibit progressively greater vertical offset, which attests to repeated Quaternary fault movements. In the same fashion, the Dry Hills fault (Figure 8) exhibits multiple Quaternary displacements, the youngest of which clearly shows Holocene surface expression.

In summary, aerial photo analysis and preliminary field studies show that fault ruptures have been most recent along the Shoshone, Dry Hills, and northern section of the Malpais fault (Figure 8), with no evidence for late Quaternary fault movements in the BGF and elsewhere along the southern Malpais fault.

Our model of stress changes associated with these most recent fault ruptures (Figure 9) suggests that the Malpais fault in the vicinity of the BGF has experienced a significant increase in failure stress on the order of 1-2 bars at 3 km depth (Figure 9a). The positive CFF values result from slip on both the Shoshone fault and the northern section of the Malpais fault. Slip on the Dry Hills fault results in negative CFF values along the southern Malpais fault. CFF values calculated for depths of 6 km yield similar results, although these calculations are not included herein.

A comparison of Figures 9a and 9b shows that CFF calculations in the BGF for a friction value of zero (Figure 9b) are less than those for a value of friction of 0.4 (Figure 9a). This indicates that the positive CFF values are a result of both increases in shear stress and decreases in normal stress. The sense of stress changes is similar to the changes in the DVGF. However, the stress changes in the BGF are considerably smaller owing to the greater distance between the geothermal field and the most recent fault ruptures.

### **Bradys Geothermal Field**

Mapping by Bell (1984) indicates that the Bradys Geothermal field lies at the endpoint of Holocene fault ruptures (Figure 10). These ruptures lie within the pluvial Lake Lahontan basin, and are therefore required to be younger than the most recent latest Pleistocene occupation of the lake. We are currently conducting detailed field studies to more completely assess the distribution and age of surface faulting, and have yet to analyze stress changes associated with the fault ruptures. Our preliminary studies indicate that the southern extent of ruptures is accurately portrayed by Bell (1984), but that the fault ruptures may extend farther to the north. These relations would indicate that the Bradys area lies in an area of pronounced stress change owing to its close proximity to a recent fault rupture endpoint. From our previous models of the DVGF we anticipate that these stress changes would result from both increases in shear stress and decreases in normal stress resolved parallel to normal slip on the fault.

### **DISCUSSION AND CONCLUSIONS**

Our models for the Dixie Valley geothermal field indicate that induced stress changes near the endpoints of recent fault ruptures appear to promote favorable conditions for geothermal production. The stress changes result in an increase in failure stress on unruptured, along-strike portions of the fault. These stress changes are also characterized by significant

decreases in fault-normal stress that are particularly enhanced in the upper few kilometers of the crust. Our models of Holocene stress changes in Dixie Valley, suggest the area between the northern- and southernmost geothermal production wells coincides with the portion of the fault most strongly affected by tensile stress changes. Stress changes in the geothermal field induced by the 1915 and 1954 earthquakes are in the same sense as in the Holocene stress model. However, these changes are smaller because of the greater distance between the geothermal field and the historic rupture endpoints. Both the Holocene and historic stress changes we calculate are consistent with results from recent investigations of in-situ stress and fracture permeability in the Dixie Valley geothermal field (e.g. Barton et. al, 1996; Hickman et al., 1997). These studies show fractures parallel to the fault zone are both critically stressed for failure and hydraulically conductive.

Our preliminary assessment of the neotectonic framework of the Bradys geothermal field indicates that this production area lies at the endpoint of a Holocene earthquake rupture, a setting that is analogous to the Dixie Valley geothermal field. We anticipate that stress models for the Bradys area will yield similar results as for the Dixie Valley geothermal field. The Beowawe geothermal field lies in a more complex structural setting. However, our model for late Pleistocene-Holocene stress changes along the southern Malpais fault shows both increases in shear stress and decreases in normal stress in the Beowawe geothermal field.

In summary, we find that the Basin and Range geothermal production fields we have investigated do not appear to lie along the most recently active portions of faults. Our studies show that induced stress concentrations at the endpoints of fault ruptures promote conditions for fracture permeability and geothermal production. . This may be accomplished in two ways: 1) Nearby fault ruptures may induce aftershocks associated with small amounts of slip on macro fractures along the fault and within the damage zone of the fault, thereby producing open fractures while maintaining high failure stress conditions on the fault; and 2) If the geothermal field is close enough to fault rupture endpoints, then it is conceivable that decreases in fault-normal stress may be large enough to produce significant increases in fracture dilatancy, thereby increasing hydraulic conductivity. The observations would suggest that in regions of high heat flow, areas along normal faults which act as persistent rupture segment boundaries may also be areas of enhanced hydrothermal activity. Studies of normal fault segmentation show that fault

trace salients (i.e. convex fault strike changes such as at the Dixie Valley geothermal field) and fault trace steps appear to act as the most persistent fault rupture boundaries (Crone and Haller, 1991; Machette et al., 1991).

Our studies illustrate that a detailed understanding of the neotectonic framework and the mechanics of faulting processes are fundamental to developing conceptual models for controls on the state of stress and fracture permeability in geothermal fields. We feel that this integrated approach has enormous potential as a geothermal exploration tool.

Our continuing efforts will focus on constraining better the absolute ages and distribution of fault ruptures in the Dixie Valley, Beowawe, and Bradys areas and on investigating the recent fault history and stress changes for geothermal production fields elsewhere in the Basin and Range province.

#### **ACKNOWLEDGEMENTS**

This study was supported by the Department of Energy's Geothermal Reservoir Technology Research, Development, and Demonstration Solicitation Program, award number DE-FG07-98ID13620. We also thank Dick Benoit for sharing his knowledge of the geology of the Dixie Valley and Beowawe areas, helpful discussions, and encouragement, John Bell for field consultations, Rich Briggs and Sheryl Fontaine for their contributions to figures and stress analyses, Nathan Smith and Mark Trevor for field assistance, and the crew at Oxbow Geothermal Corp. for all the help and good cheer they provided during the hot summer field season in Dixie Valley.

#### **REFERENCES**

- Barton, C.A., Zoback, M.D., and Hickman, S.H. (1996), Critically stressed faults and fluid flow in crystalline and sedimentary rock, analysis of localized stress perturbations and thermal anomalies, *EOS Transactions*, **77**, p. F228.
- Bell, J.W. (1984), Quaternary fault map of Nevada, Reno Sheet, Nevada Bureau of Mines and Geology Map 79.
- Bell, J., and Katzer, T. (1990), Timing of late Quaternary faulting in the 1954 Dixie Valley earthquake area, central Nevada., *Geology*, **18**, 622-625.

- Benoit, D. (1995), Forced folding and Basin and Range geothermal systems, *Geothermal Resources Council Transactions*, **19**, 155-163.
- Berry, G. W., Grim, P. J., Ikelman, J. A. (1980), Thermal springs list for the United States: National Oceanic and Atmospheric Administration Key to Geophysical Records Documentation 12, National Geophysical and Solar-Terrestrial Data Center, Data Mapping Group, Cod D64, Boulder, 59 p.
- Byerlee, J. (1978), Friction of rocks, *Pageoph.*, **116**, 615-626.
- Caskey, S.J., Wesnousky, S.G., Zhang, P., and Slemmons, D.B. (1996), Surface faulting of the 1954 Fairview Peak (Ms7.2) and Dixie Valley (Ms6.8) earthquakes, central Nevada: *Bull. Seism. Soc. Am.*, **86**, 761-787.
- Crone, A. J. and Haller, K. M. (1991), Segmentation and the coseismic behavior of Basin and Range normal faults: examples from east-central Idaho and southwestern Montana, U.S.A., *Journal of Structural Geology*, **13**, 151-164.
- Dohrenwend, J. C., Schell, B. A., Menges, C. M., Moring, B. C., McKittrick, M. A. (1996). Reconnaissance photogeologic map of young (Quaternary and late Tertiary) faults in Nevada, Nevada Bureau of Mines and Geology Open-File Report 96-2, prepared in cooperation with the U.S. Geological Survey.
- Hickman, S.H., Barton, C.A., Zoback, M.D., Morin, R., Sass, J., and Benoit, R. (1997), In-situ stress and fracture permeability along the Stillwater fault zone, Dixie Valley, Nevada, *Int. J. Rock Mech. & Min. Sci.*, **34**, 3-4.
- Machette, M. N., Personius, S. F., Nelson, A. R., Schwartz, D. P., and Lund, W. R. (The Wasatch fault zone, Utah-segmentation and history of Holocene earthquakes, *Journal of Structural Geology*, **13**, 137-149.
- Okada, Y. (1992), Internal deformation due to shear and tensile faults in a half-space, *Bull. Seism. Soc. Am.*, **82**, 1018-1040.
- Pearthree, P.A. (1990), Geomorphic analyses of young faulting and fault behavior in central Nevada [Ph.D. thesis]: University of Arizona, 212 p.
- Reasenberg, P. A. and Simpson, R. W. (1992), Response of regional seismicity to the static stress change produced by the Loma Prieta earthquake, *Science*, **255**, 1687-1690.
- Smith, C., Struhsacker, E. M., and Struhsacker, E. W. (1979), Structural inferences from geologic and geophysical data at the Beowawe KGRA, north-central Nevada, *Geothermal Resources Council, Transactions*, **8**, 451-456.
- Stein, R. S., King, G. C. P., and Jian, L. (1992), Change in failure stress on the southern San Andreas fault system caused by the 1992 Magnitude=7.4 Landers earthquake, *Science*, **258**, 1328-1332.
- Stewart, J. H. and Carlson, J. E. (1978), Geologic Map of Nevada, prepared by the U.S. Geological Survey in cooperation with the Nevada Bureau of Mines and Geology.
- Wallace, R. E. (1984), Fault scarps formed during the earthquakes of October 2, 1915, in Pleasant Valley, Nevada, and some tectonic implications, *U. S. Geol. Surv. Prof. Pap. 1274-A*, 1-33.
- Wallace, R.E., and Whitney, R.A. (1984), Late Quaternary history of the Stillwater seismic gap, Nevada, *Bull. Seism. Soc. Am.*, **74**, 301-314.

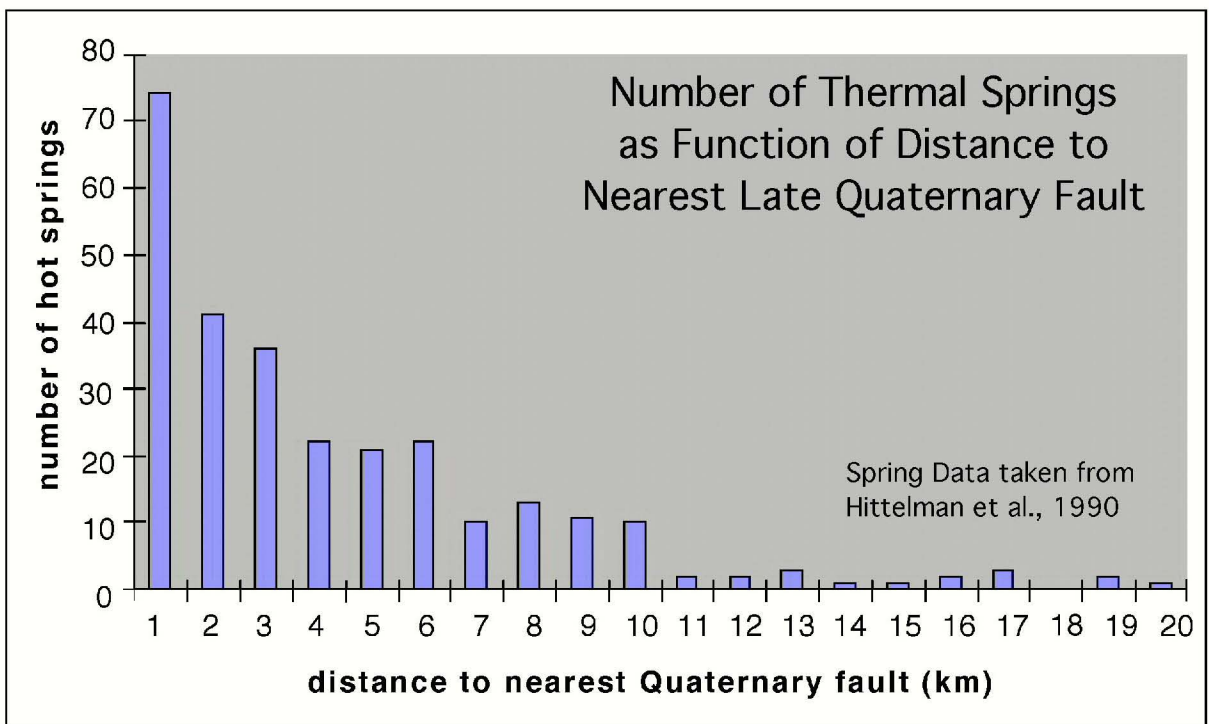


*Figure. 1. Number of thermal springs as a function of distance to the nearest late Quaternary fault.*

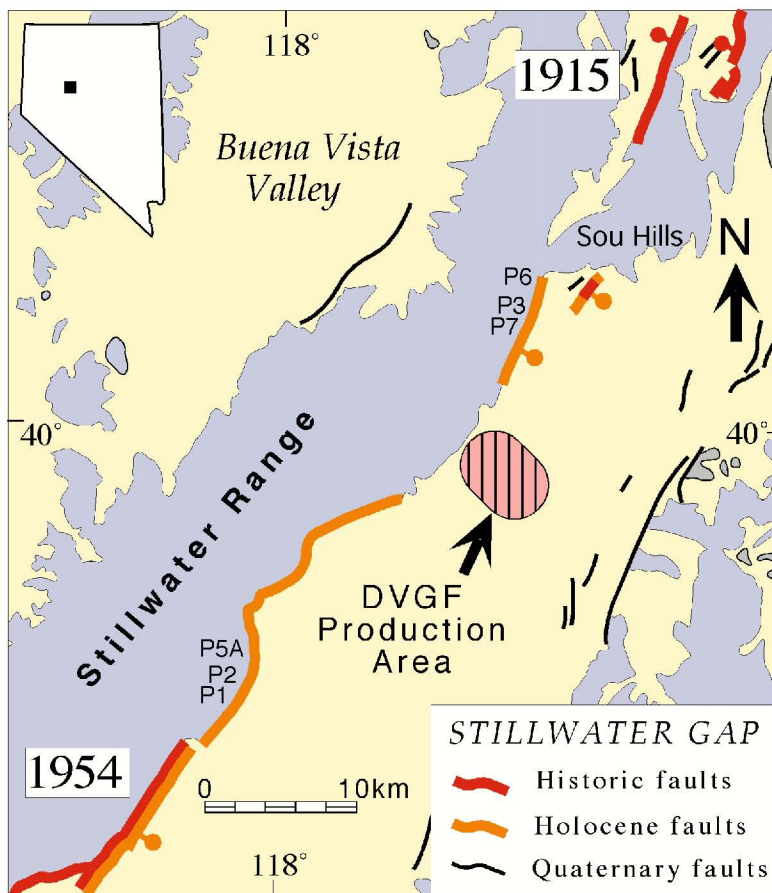


**Figure. 2. Generalized fault map of the Stillwater Gap area showing the distribution of historic 1915 and 1954 ruptures (bold red lines), Holocene ruptures (bold orange lines) and Quaternary faults (thin black lines). Base map (modified after Stewart and Carlson, 1978) shows distributions of bedrock (gray) and Quaternary alluvium (yellow). Map also shows the area of the Dixie Valley geothermal field (DVGF). Areas labeled P1-P7 correspond to locations of scarp profiles shown in Figure 3.**

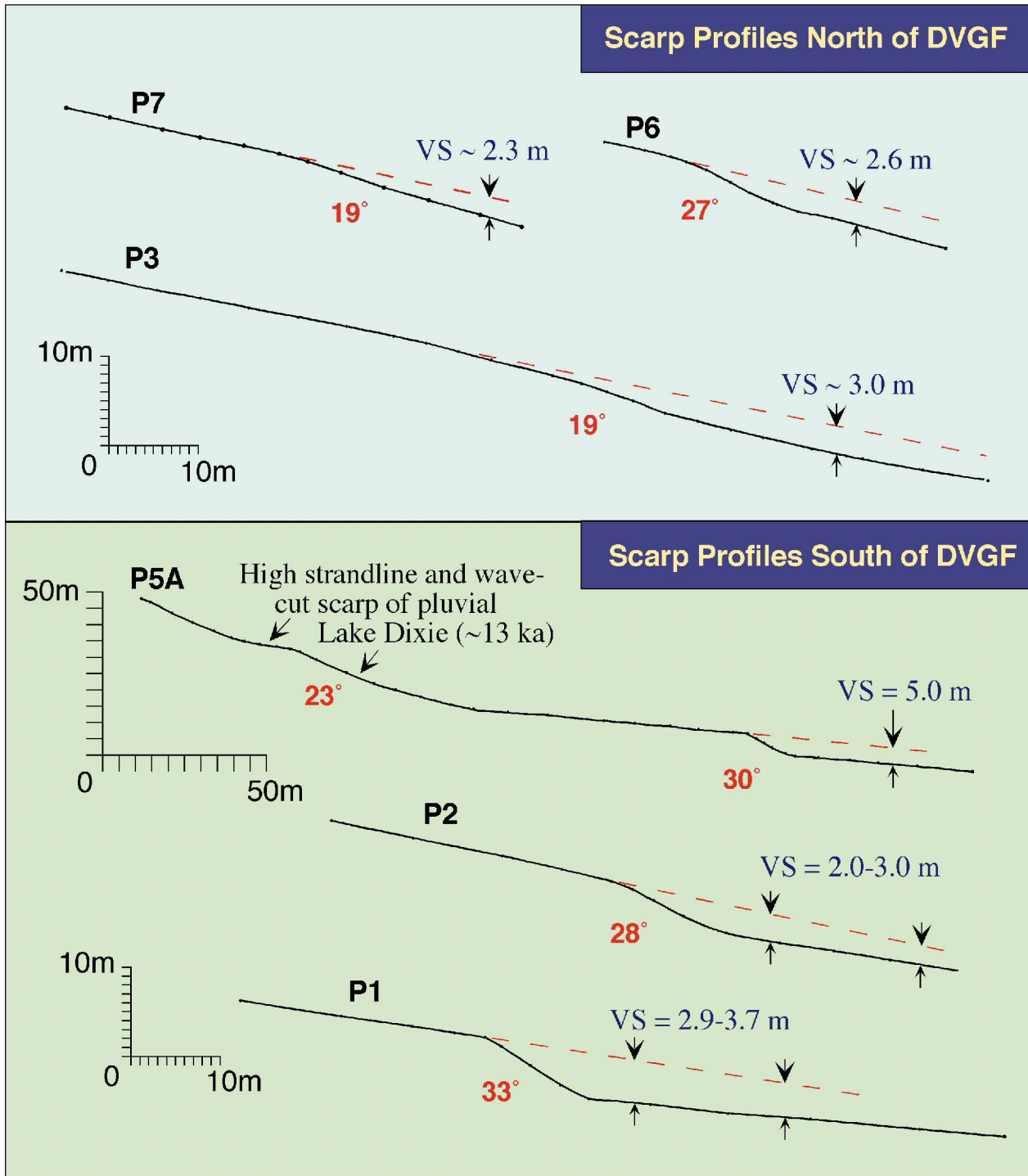


**Figure 3. Representative fault scarp profiles across Holocene fault ruptures north and south of the Dixie Valley geothermal field. Profile locations are shown on Figure 2. Scarp slope angles are shown below profiles.**

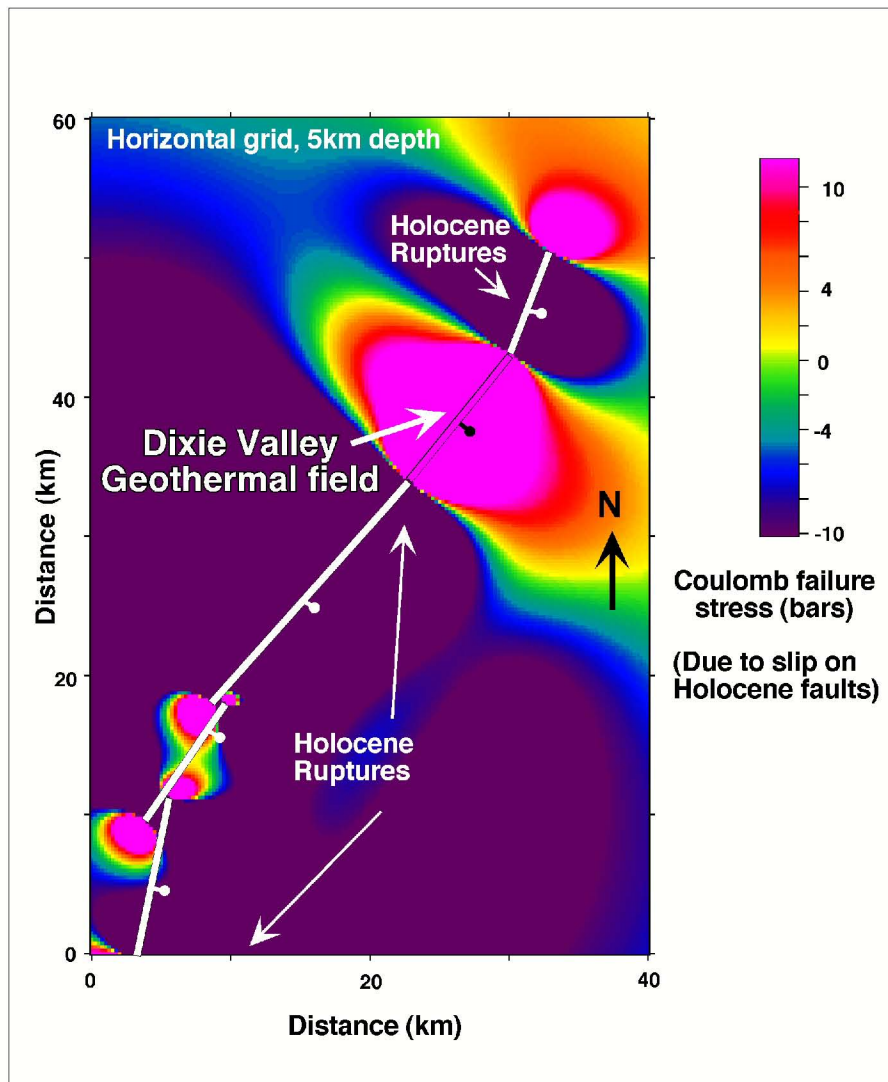


**Figure. 4.** *Coulomb failure stress changes in the DVGF associated with Holocene fault ruptures along the Dixie Valley fault. Calculations are shown on a horizontal grid at 5 km depth, for friction coefficient for 0.75 and resolved on  $040^{\circ} 50SE$  oriented normal fault planes (same as Dixie Valley fault in the DVGF) along a  $-90^{\circ}$  rake (dip slip direction of slip). White dislocations represent active slip surfaces. For the fault segments south of the DVGF, we assign values of dip slip of 1.56 m, 2.12 m, and 3.92 m (south to north) based on field measurements of vertical offset across fault scarps. Similarly we assign a dip slip value of 1.96 m for the dislocation north of the DVGF. The transparent dislocation represents the section of the Dixie Valley fault that lies between the Holocene rupture segments.*

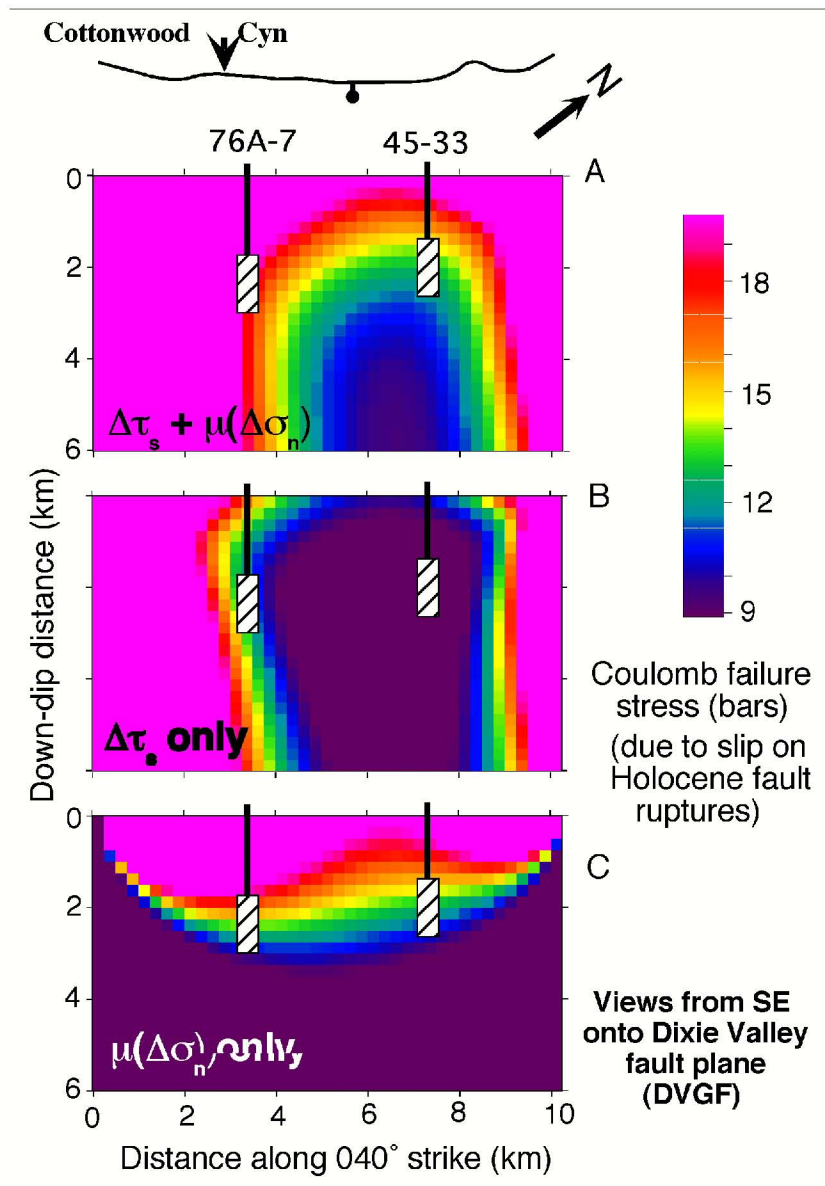
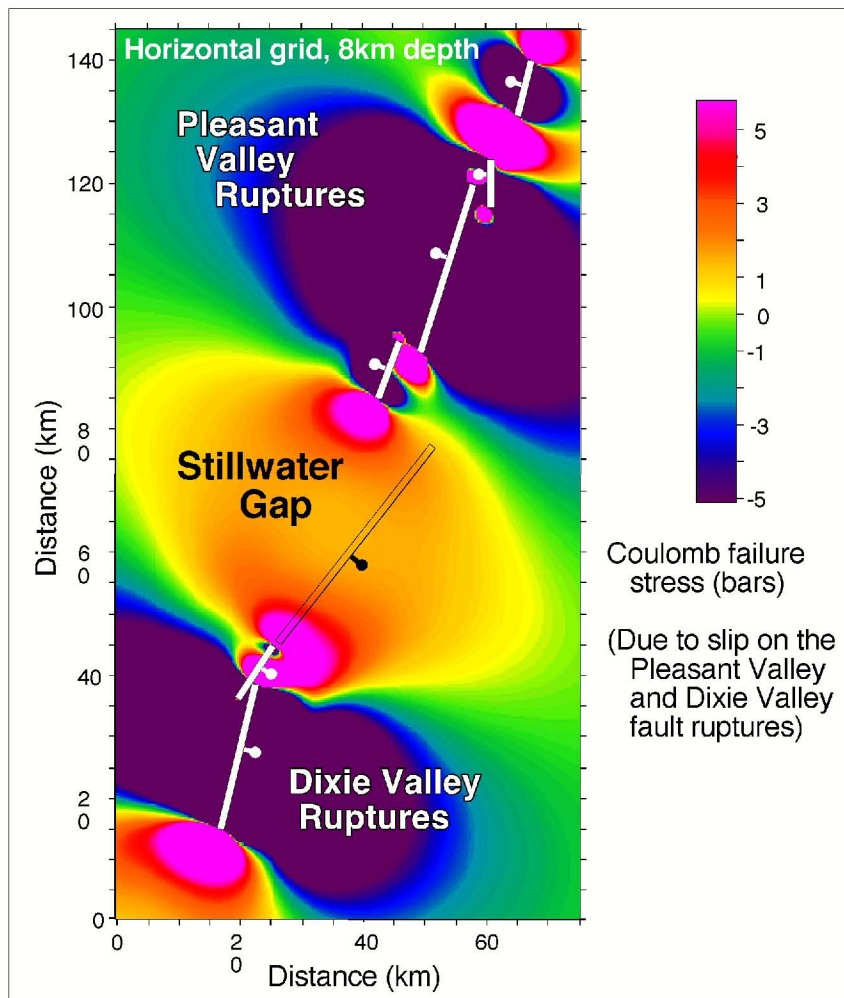


Figure. 5. Coulomb failure stress changes from Holocene fault ruptures resolved on the Dixie Valley fault in the area of the DVGF for down-dip distances of 6 km. Views are perpendicular to the fault plane as viewed from the southeast. Figures show contributions of CFF from; A) changes in shear and normal stress, B) changes in shear stress only, and C) changes in normal stress only. Stress changes are resolved along a  $-90^\circ$  rake (dip slip direction of slip). The map trace of this segment of the Dixie Valley fault is shown above the plots for reference. 76A-7 and 45-33 denote locations of the northern- and southern-most production wells in the DVGF



*Figure. 6. Coulomb failure stress changes in the Stillwater Gap associated with slip on the 1915 Pleasant Valley and 1954 Dixie Valley earthquake ruptures (shown as white dislocations). Slip on the dislocations is constrained from detailed field studies of fault slip (Caskey et al., 1996; Wallace, 1984). Transparent dislocation represents the Stillwater Gap portion of the Dixie Valley fault. Calculations are shown on a horizontal grid at 8 km depth, for a friction coefficient of 0.75 and resolved on  $038^{\circ} 50SE$  oriented normal fault planes (same as Dixie Valley fault in the Stillwater Gap) along a  $-90^{\circ}$  rake (dip slip direction of slip).*

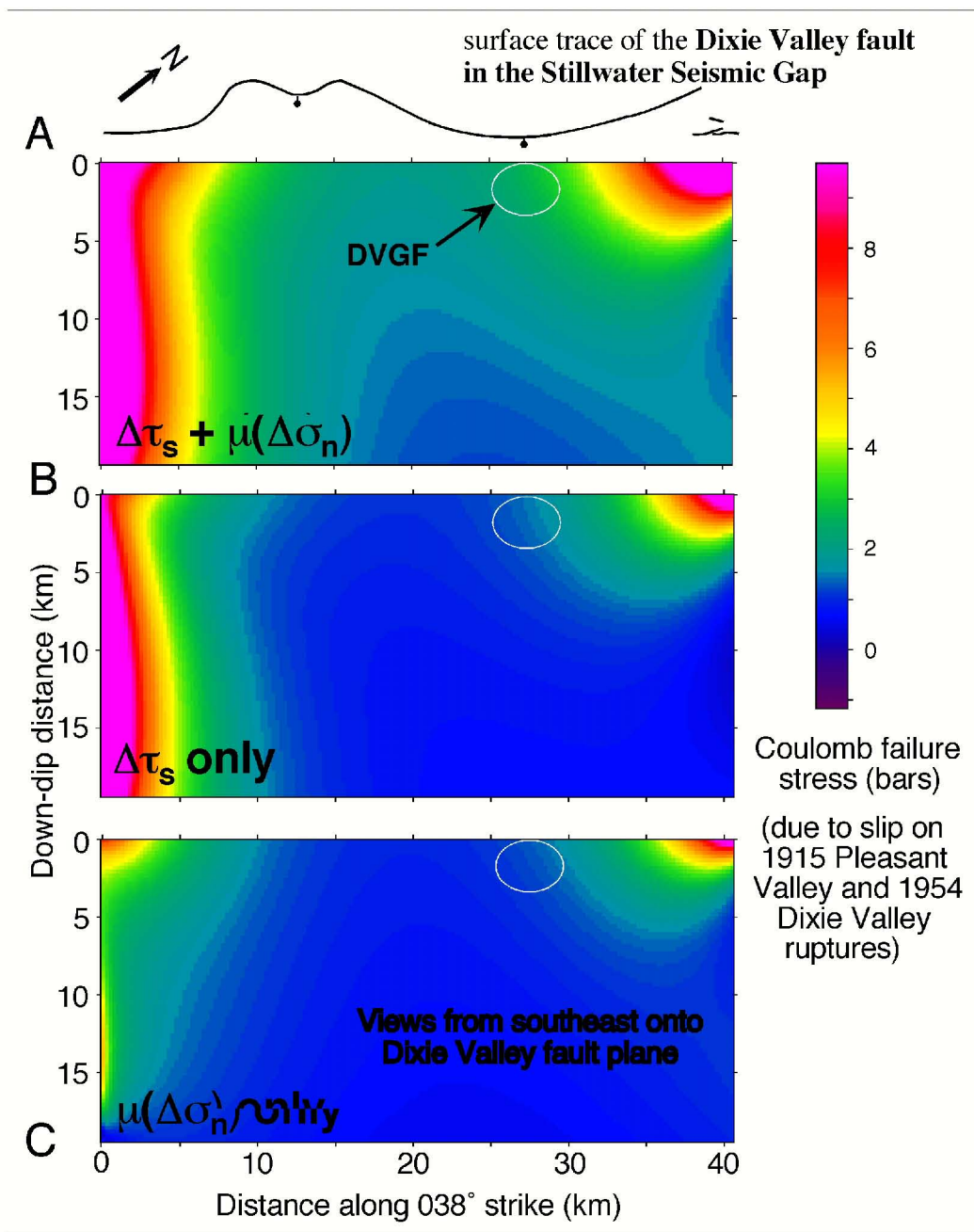
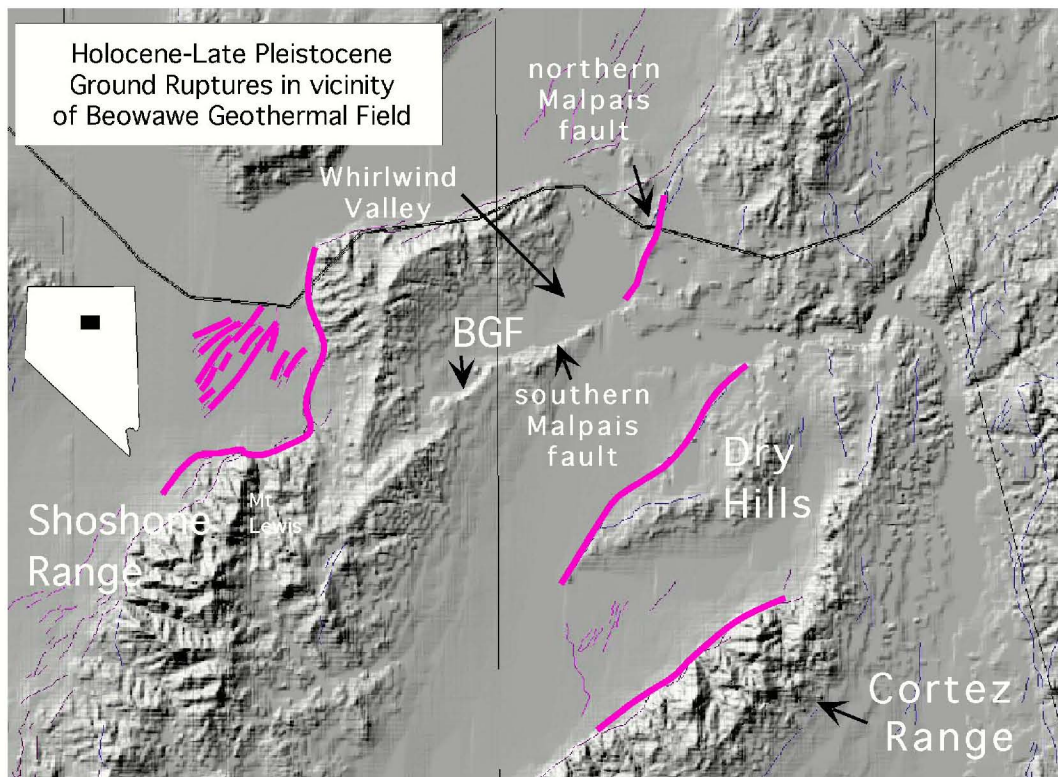
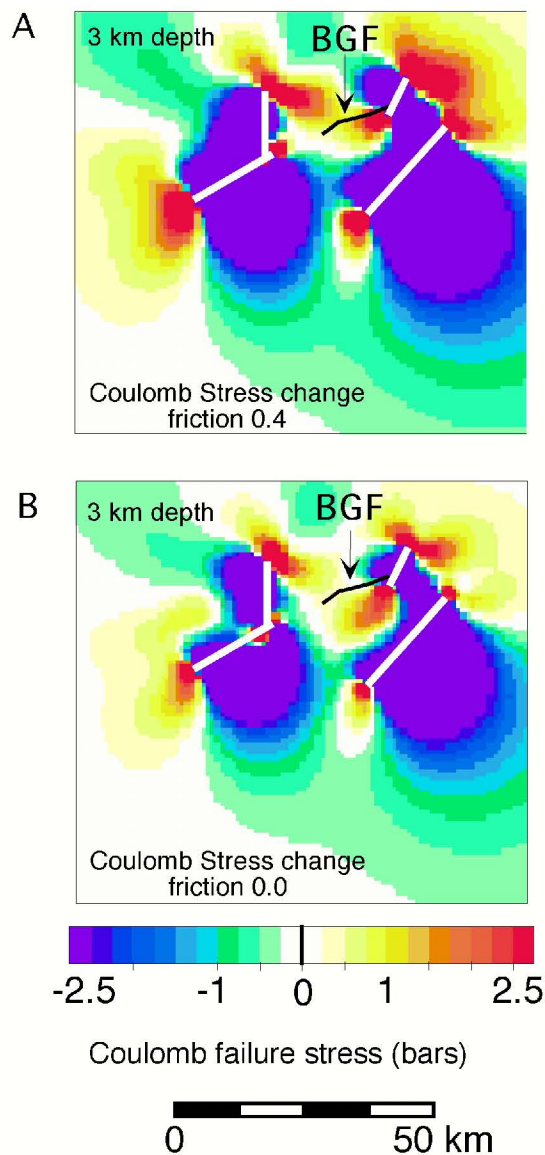


Figure 7. Coulomb failure changes from historic fault ruptures resolved on the Dixie Valley fault in the Stillwater Gap for down-dip distances of  $\sim 19$  km. Views are perpendicular to the fault plane as viewed from the southeast. Figures show contributions of CFF from; A) changes in shear and normal stress, B) changes in shear stress only, and C) changes in normal stress only. Stress changes are resolved along a  $-90^\circ$  rake (dip slip direction of slip). Map trace of the Stillwater Gap segment of the fault is shown above the fault plane view for reference.



*Figure. 8. Location map of the Beowawe geothermal field (BGF) showing the traces of the most recent fault ruptures along the west flanks of the Shoshone Range and the Dry Hills, and the northern Malpais fault. These fault ruptures are used for the stress analysis of the BGF (Figure 9).*



*Figure. 9. Coulomb failure stress changes at 3 kms depth in the Beowawe geothermal field (BGF) associated with the most recent fault ruptures (white dislocations) in the area. We assign 1.0 m of dip slip on each of the rupture segments along the Shoshone Range, Dry Hills, and northern Malpais fault based on field measurements of vertical offset across the faults. Black dislocation represents the southern Malpais fault. Calculations are for friction coefficient for; A) 0.40, and B) 0.0. Stress is resolved on planes oriented  $245^{\circ} 60\text{NW}$  (same as southern Malpais fault) along a  $-90^{\circ}$  rake (dip slip direction of slip).*

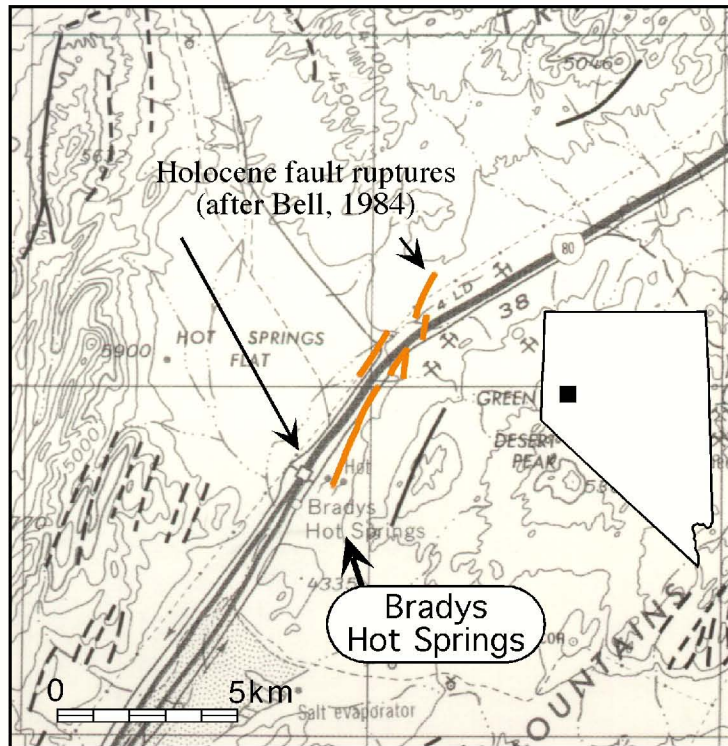


*Figure. 10. Location map of the Bradys geothermal field showing previously mapped Holocene fault trace (base map modified after Bell, 1984).*